ADVANCED MATERIALS TECHNOLOGIES
www.advmattechnol.de

Highly Sensitive, Low Voltage Operation, and Low Power Consumption Resistive Strain Sensors Based on Vertically Oriented Graphene Nanosheets

*Qianqing Jiang, Chengchun Tang, Huaping Wang, Jie Yang, Junjie Li, Changzhi Gu, and Gui Yu**

Flexible and stretchable electronics are essential module of mobile wearable devices, soft human–machine interfaces, and also e-skin on biomedical prostheses and biorobotics. Strain sensors, as one of the major part of flexible electronics, have been extensively studied recently. When being used for mobile and long-term applications, low power consumption and low operation voltage beside high sensitivity and fast response of the sensors are required. Easy integration is also an important aspect to build an internet of things. Here, resistive strain sensors with a maximum gauge factor of 150, a fast response time of about 10 ms, a low operation voltage of 20 mV, and a low power consumption of <8 µW, are demonstrated by introducing easily patternable vertically oriented graphene nanosheets (VGs film) as the sensing material. Ultrasmall strain of 0.07% can be detected with VGs film patterned into 200 µm × 200 µm square array. It is the special structure of the VGs film with a combination of an underlying buffer layer and vertically oriented nanosheets upon it that ensures both the high sensitivity and the low power consumption. To demonstrate the capacities of the sensor, the sensor was applied to monitor the human artery pulses.

Dr. Q. Jiang, Dr. H. Wang, J. Yang, Prof. G. Yu
Beijing National Laboratory for Molecular Sciences
CAS Research/Education Center for Excellence in Molecular Sciences
Institute of Chemistry
Chinese Academy of Sciences
Beijing 100190, P. R. China
E-mail: yugui@iccas.ac.cn

C. Tang, Prof. J. Li, Prof. C. Gu
Beijing National Laboratory for Condensed Matter Physics
Institute of Physics
Chinese Academy of Sciences
Beijing 100190, P. R. China

C. Tang
Institute for Quantum Science and Engineering
Department of Physics
Southern University of Science and Technology
Shenzhen 518055, P. R. China

Prof. G. Yu
School of Chemical Sciences
University of Chinese Academy of Sciences
Beijing 100049, P. R. China

The ORCID identification number(s) for the author(s) of this article can be found under https://doi.org/10.1002/admt.201800572.

DOI: 10.1002/admt.201800572

Stretchable sensors, including integration of traditional sensors on soft substrates and direct employment of stretchable sensitive materials, have attracted much attention from both researchers and engineers recently. Among them, the strain and pressure sensors for transverse stretch and vertical compression have shown promising potential in applications in fields such as electronic skin, electronic fabrics, human–computer interface, and health care.[1–6] As the strain and also the pressure sensing are mainly based on the deformation of the sensitive material, they are often detectable with in-equable sensitivity by a single device.[7] A strain or pressure sensor can signify micromovement of muscles such as the voice, artery pulses, and facial expressions, which makes it possible for health monitoring, medical diagnosis, and even assistance of drug delivery.[8–12] Metal and semiconductor materials are commonly used for strain sensors. The metallic strain sensors are restricted by low sensitivity while the semiconductor ones have thermal effect and resistive drift during the stretching process, which limits the sensor resolution.

Graphene and carbon nanotubes, known for their excellent mechanical property and thermal stability, have provided better choices for strain sensors and been extensively studied.[13–19] It has been shown that, single layer graphene is not sensitive enough to strains. It is often used as function layers to structure strain sensors which makes the fabrication process much more complicated.[13,14] A great deal of other graphene related materials have then been explored. Graphene overlaps,[15–17] quasi-3D graphene films,[20,21] and polymers incorporated with graphene[22–24] are among the most studied to construct strain sensors. Better device performance has been achieved with them. However, building a high-performance strain sensor based on graphene for practical utilization is still a big challenge.

Structure modification is a commonly applied method to enhance the device performance for the materials mentioned above. Properties such as the sensitivity and signal-to-noise ratio (SNR) can be improved this way. Model-transferring, benefiting from the advantages of simplicity, low cost, and time

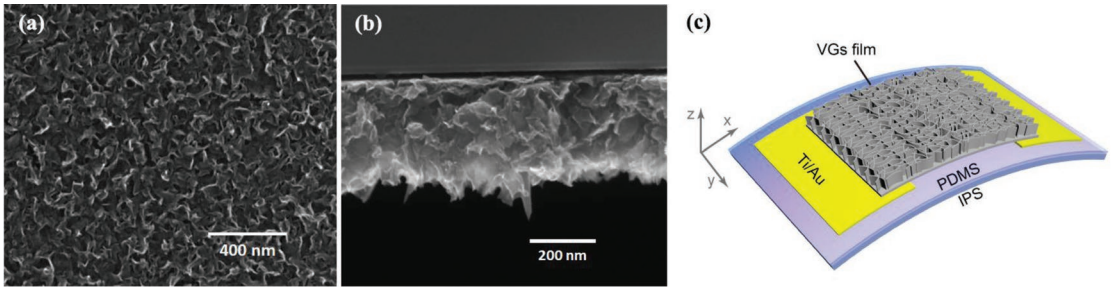

Figure 1. Strain sensor based on VGs films. SEM picture of VGs film grown on Si substrate, a) taken at top view and b) at the cross-section. c) Schematic illustration of the device structure.

conserving, are among the most referred patterning methods. Cu meshes,[7,25] poly (methyl methacrylate) (PMMA) film patterned with computer numerical control milling process,[26] polydimethylsiloxane (PDMS) stamp patterned with photoresist mold on silicon wafer,[27] and so on, have been used as the patterning molds. Processes such as chemical vapor deposition (CVD) growing of graphene[7,25] or dipping of graphene nanoplatelet dispersion[26] are then taken. Limited to the morphology of the templates, the formed patterns are usually patch arrays or connected meshes. Other patterning methods including reactive ions etching (RIE) and stamping techniques,[28] laser scribe,[29] stretch–shrink process,[30] and so on, have also been reported. Most of the methods can result in a characteristic cell size larger than 200 μm. For integration and application where the device size is severely restricted, taking microrobots as an example, smaller device size might be needed. The RIE technique is then preferable in this perspective, as very small etching masks can be prepared with lithography before the RIE patterning. However, this process is not quite suitable for sensors built with thick graphene materials and graphene-polymers incorporated films. A lithography compatible film with good sensing performance is then in need.

On the other hand, in mobile and long-term operation applications, taking real-time health monitoring as an example, low power consumption and low-voltage operation beside high sensitivity and fast response are of crucial importance. These two properties are also very important for the building of an all wearable monitoring system, as the emerging wearable energy supplies always have a quite low efficiency. RF energy,[31] light,[32] body heat,[33] body motion,[34] and also human sweat[35] have been reported as energy sources for wearable devices. Except the light, the mentioned energy sources provide a quite small power density with a typical value of 100 μW cm^{-2}. Sensor devices with high energy consumption cannot be well supported by them. It is then of obvious importance for the sensor devices to realize a low power consumption.

Here, we present a new strain sensor with low voltage operation (20 mV) and low power consumption (<8 μW) built by CVD-grown vertically oriented graphene nanosheets with some underlying continuous graphene layers (referred to as VGs film), which is lithography and RIE process compatible. Benefiting from its individual structure, the VGs film showed a very low square resistance of 93.45 Ω $\square^{-1}$ which makes it good for electrical conductivity and further reduces the power consumption of the sensor device. Besides, the standing nanosheets are the basis of high responsivity to applied strain of the sensors and excellent strain response characteristics can be obtained with a patterning process of the film. Gauge factor of 150 was obtained from patterned VGs ribbons and the detectable strain can reach as small as 0.07% with a 200 μm × 200 μm VGs square array. Very fast response time as low as 10 ms was achieved, which makes it possible to capture quick movements of muscles or test small fluctuation of blood vessel for the sensors. We finally demonstrated the capacities of the VGs film sensor by measuring radial artery pulses which showed its ability in daily health monitoring.

As mentioned above, VGs films were chosen as the strain sensitive element for our sensor device. The films were prepared on Si or SiO_2 substrate with a thermal CVD method.[36,37] Films with high-density nanosheets were used in our experiments (**Figure 1**a). Special layered texture of the films containing some underlying continuous buffer layer and also vertically oriented graphene sheets of about 100–300 nm in height upon the layers had been verified with varied methods. Scanning electron microscope (SEM) picture taken at cross section of VGs film grown on a Si substrate is shown in Figure 1b. Pieces of nanosheets contacting each other can be clearly seen in the picture, while the forming of the underlying buffer layer was confirmed by Raman spectra and SEM images at various growing stages of the VGs film.[36]

The basic structure of our sensor device is shown in Figure 1c. Upon the impact-resistant polystyrene (IPS, purchased from Obducat) substrate, a PDMS (Sylgard 184 purchased from Dow Corning) layer was formed with a "spin-coating and curing" process. Ti/Au electrodes were deposited on the PDMS/IPS substrate and VGs film was then carefully placed to connect the two ends of the electrodes. The VGs film contacted the PDMS layer out of the electrodes and good attachment of the film to the substrate was then achieved. For clear expression, the *x*- and *y*-directions is defined as shown in Figure 1c. More details on the device fabrication can be found in Figure S1 in the Supporting Information.

Device performance was then tested under strain applied along the *x*-direction with a home-built move controller which was connected to Keithly 4200 for the electrical measurement. Details of the test scheme are discussed in Note S1 and Figure S2 in the Supporting Information. As positive effects of film patterning were observed in the experiments, we focused mainly on the devices built with patterned VGs films. As a contrast, resistive responding characteristics before and after patterning of the PMMA-covered VGs film on a sensor device are given in **Figure 2**a. Metal etch-mask and RIE (Plasma Lab

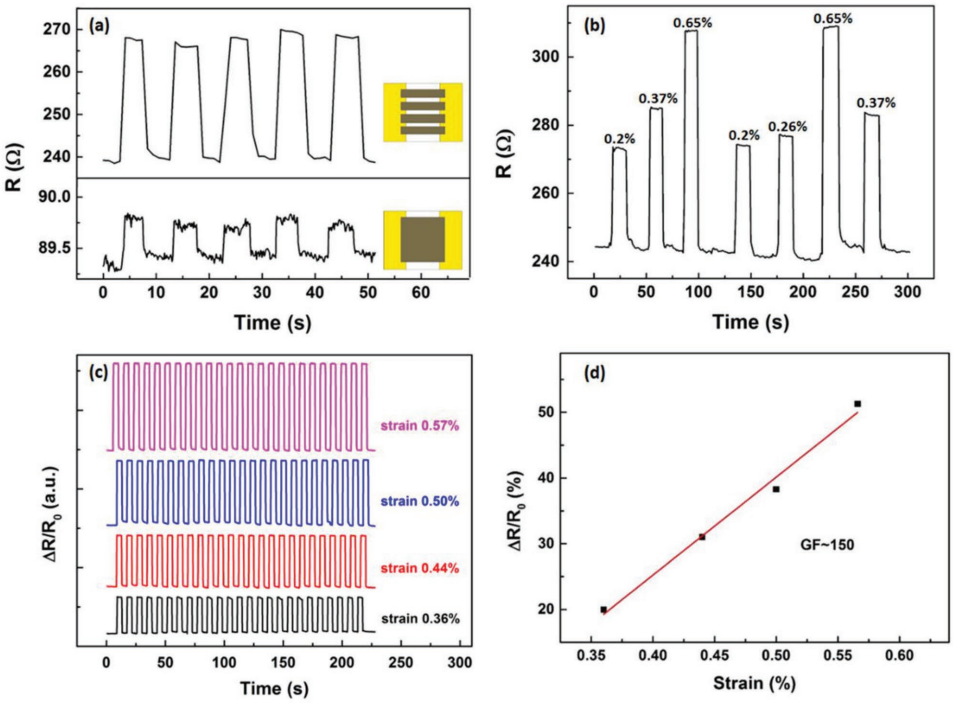

Figure 2. Performance of strain sensors based on VGs films patterned into four ribbons a,b) with and c,d) without PMMA cover. a) The resistance response of device based on unpatterned VGs film under strain of 0.37%, and patterned VGs ribbons under strain of 0.25%. Insets: the sensor device before and after patterning of the VGs film. b) Resistance response of the device based on patterned VGs ribbons to varied strain. The fitted S_{GF} is about 42. c) Resistance response of device based on patterned VGs ribbons without PMMA layer under strain of 0.36%, 0.44%, 0.50%, and 0.57%. d) Relative change of the resistance as a function of the strain load. The red is the fitted line by linear approximation and the gauge factor is about 150.

80 Plus, Oxford Instruments Company) system were used in the patterning of VGs film. Etching parameters of pressure = 100 mTorr, O_2 = 50 sccm, power = 100 W were applied. Before patterning the VGs film, the device showed a low resistance of about 89.5 Ω without any strain load. Increasing the strain load to 0.37% resulted in a resistance increase by 0.33%. After being patterned into four parallel ribbons with a width of about 1 mm and a 1 mm wide gap between each ribbon, original resistance of the device increased from 89.5 to 237 Ω. Clearly distinguishable resistance responses under different strain are plotted in Figure 2b. An obvious increase in resistance response sensitivity was obtained with the device due to the VGs film patterning. It should be mentioned that, for etched ribbons, direction parallel to the ribbons was defined as *x*-direction, along which the strain was applied in the measurement.

For quantization, sensitivity of strain sensors can be expressed by the gauge factor, S_{GF}, which is defined as $\Delta R/R_0 = S_{GF} \times \varepsilon$, where $\varepsilon = \Delta L/L_0$ demonstrates the degree of strain with L_0 representing the original length of the sensitive material in the stretching direction and $\Delta R/R_0$ demonstrates the relative change of device resistance with R_0 representing the original resistance. By a linear approximation, the calculated S_{GF} of the device was enhanced from 0.9 to 42 by patterning the VGs film.

In another PMMA-free case, the VGs film was also patterned into four parallel ribbons which are same with the PMMA-covered one discussed above. Device response is shown in Figure 2c. A high S_{GF} of 150 which was much larger than the average value of unpatterned devices was obtained (Figure 2d). Similarly, the sensor device based on un-patterned VGs film without PMMA layer showed a low S_{GF} of 2.3 (Figure S3, Supporting Information). These results indicated that the PMMA covered layer can lead to a decrease of S_{GF} value while patterning VGs film into ribbons is favorable to the enhancement of S_{GF}. We suppose that the covering PMMA layer on VGs films may limit the deformation of VGs under applied strain and result in low strain response characteristics of the devices. So the following discussion is all taken based on sensor devices without the covered PMMA layer. It has been furtherly confirmed on a typical device that, response to strain along the *x*-direction is more sensitive than that along the *y*-direction. The sensor is not only sensitive to uniaxial stress, but it is most sensitive to stress along the *x*-direction (Figure S4, Supporting Information).

In order to confirm the contribution of the standing nanosheets to resistance response of the strain sensor, devices based on VGs films with different standing nanosheet density were fabricated (Figure S5, Supporting Information). According to our experiments, devices built with plane graphene film or VGs film with low-density nanosheets showed poor or even no response to applied strain. In a certain range, the performance of the sensor devices improved with the increasing of the nanosheets density. It can be then determined that the standing nanosheets were the basic condition for normal performance of the devices built with VGs films.

The improvement of the device performance resulted from the film patterning process can be mainly contributed to the introduced ribbon edges. Lateral etching of VGs film existed

when it being patterned with metal etch masks in the O_2 plasma etching process.[38] It resulted in a width shrink of the prepared ribbons. In our etching system, with a 200 μm wide Mo etch mask, the prepared VGs ribbon was about 180 μm in width. It indicates that the energetic ions can reach about 10 μm far from the mask edge to the ribbon center. SEM images clearly show a gradual change in the morphology of the VGs film in this region (Figure S6, Supporting Information). It can be concluded from these images that, the nearer to the ribbon center, the lighter the VGs film was etched. Small cracks can then be introduced to the underlying buffer layer at certain positions around the newly formed edges this way, especially at the grain boundaries and other defect locations. And also, neighboring nanosheets at the ribbon edges can be freed from the firm bonds formed during their growth and come into random connections to each other (Figure 1b). The connection areas between these nanosheets, and furtherly the device conductance, then reduce obviously under strain.

For further analysis, a single ribbon can be divided into two parts: the edges along the stretching direction and the central part, connected in parallel. The resistance of the central part can be defined as R_c, and resistance of the edges, R_e. Then the total resistance (R) can be expressed as

$$1/R = 1/R_c + 1/R_e \quad (1)$$

For ribbons wider than 100 μm, it is reasonable to assume that, the width of the central part, W_c, is much larger than sum of the width of the two edge area along the stretching direction, W_e. Then R_e should be larger than R_c: $R_c < R_e < \infty$. We can finally get that

$$R_c/2 < R < R_c \quad (2)$$

It implies that, relative resistance change of the device caused by strain load will not be larger than 50%. Taking the deformation of the central part into consideration, results of our experiments well matched the analysis above.

As the introduction of new edges did favor to the sensor device performance, it is of significant interest to try narrower ribbons which may offer much more edges within the same film area. We first built a typical sensor device with a VGs film of about 0.7 cm × 0.7 cm in size and then patterned the film into ribbons with a width of 200 μm and a gap of 400 μm between the nearest neighbors (Figure S7, Supporting Information). Interdigital electrodes were used to fabricate sensor devices to ensure good connection between the VGs ribbons and the electrodes (**Figure 3**a, inset). Placed on such electrodes, every single VGs ribbon was divided into several small segments and these segments connected with each other in a parallel way. The original *I–V* curve of the device without applied strain is shown in Figure 3a, revealing a resistance of about 61 Ω. Resistance response to strain of 0.13%, 0.15%, and 0.19% along the ribbons are presented in Figure 3b. This sensor device showed a low detection limit of 0.13%.

To further reduce the detection limit of the strain sensor, VGs film on a sensor device was etched into an array of small squares with each of 200 μm × 200 μm in size (Figure 3c; Figure S8, Supporting Information). S-shaped electrodes had been prepared on the PDMS/IPS substrate in advance to offer serial electrical connection of the small patches. Resistance responding to strain of the device is shown in Figure 3d. Compared with the VGs ribbon sample in parallel connection

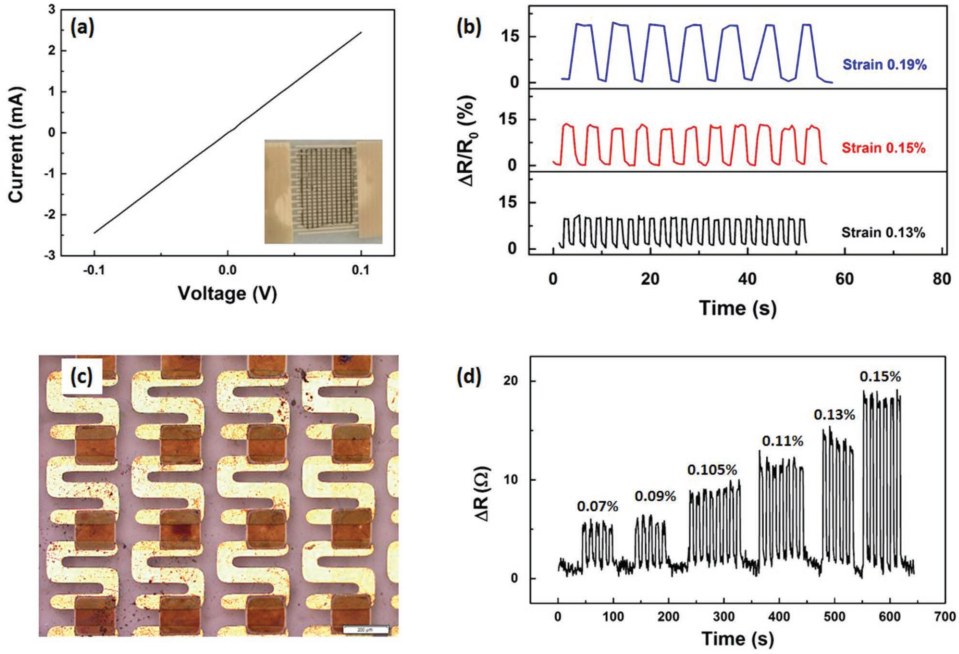

Figure 3. Electric performance of strain sensors prepared with VGs films patterned into a,b) 200 μm wide ribbons and c,d) 200 μm × 200 μm square array. a) Original *I–V* curve with no strain load of the VGs ribbons. Inset: optical image of the device with patterned VGs ribbons. b) Resistance response of the device with 200 μm wide ribbons under varied strain. The gauge factor is about 73. c) Optical microscope photo of the strain sensor based on 200 μm × 200 μm VGs square array. d) Resistance change of the square array device under varied load of strain.

discussed above, this small patch sample showed even higher sensitivity to tiny strains. Along the *S*-direction, the minimum detectable strain reached as low as 0.07%, which is among the best reported values of strain sensors based on graphene related materials.[39,40] With such a high sensibility to small strain, the sensor device has obvious advantages in tiny strain signal detection. Taking all the results of our VGs film patterning experiments into consideration, it is quite clear that with more edges etched, the sensor device could have a smaller strain detection limit. As for the sensitivity, thinner ribbons might perform better. Resistance response to varied strain of VGs ribbons with different width can be found in Figure S9 in the Supporting Information. It should be mentioned that, morphology of the VGs film itself and the ribbon number of the sensor devices also affect their performance.

Moreover, the 200 μm × 200 μm patches patterned in RIE system implies an easy integration of the VGs film sensors to more complicated systems. As a further demonstration, 50 μm wide VGs ribbons was fabricated with lithography and RIE technique (Figure S10, Supporting Information). Interdigital electrodes had been developed upon the ribbon. Sensor device with a size smaller than 1 μm can be prepared with this method in principle, which can enable its applications under certain size limitation.

Stability, response speed and power consumption are among the most important parameters for strain sensors in practical applications. The responding stability of our VGs film sensor was measured by periodically changing the strain on the four ribbons etched device (without PMMA layer) using a high-precision stepper motor. The resistance change was monitored with Keithley 4200 at a constant voltage of 20 mV. Results are given in **Figure 4**a. Repeated strain cycling about 1000 times was taken to investigate the sensor stability. Details of the resistance responses are also shown in the inset part of Figure 4a. After hundreds of test cycles, resistance of the device changed little both in the released state and the stretched state. To check the long term durability of our device, the resistance monitoring in response to applied strain of 0.37% lasting more than 15 h without interrupt has been taken on an unpatterned device. Figure S11 (Supporting Information) shows more than 10^4 recorded testing cycles in the long term measurement and also the details of the last testing cycles. These results showed that the VGs material has a certain durability.

With the stepper motor being operated at a high speed, the response time to both the strain loading and releasing processes was tested. A typical time-resolved resistance response curve of a 50 μm wide ribbon array sensor (without PMMA layer) is shown in Figure 4b. It takes about 10 ms for the device to fully transform its resistance state with the loading or unloading of strain, which is in the same range of the response time of human skin to external stimuli. More experiment results showed that the responding speed differs little between different devices. As the resistance response to applied strain mainly generated from the newly formed edges, this fast response can be contributed to the fast behavior of the nanosheets in the contact and separation cycles. It should be mentioned that, when the stepper motor moves in a low speed, lower than the speed of the resistance state transformation, the resistance–time curve will evolve gradually without steep steps, as shown in the inset part of Figure 4a.

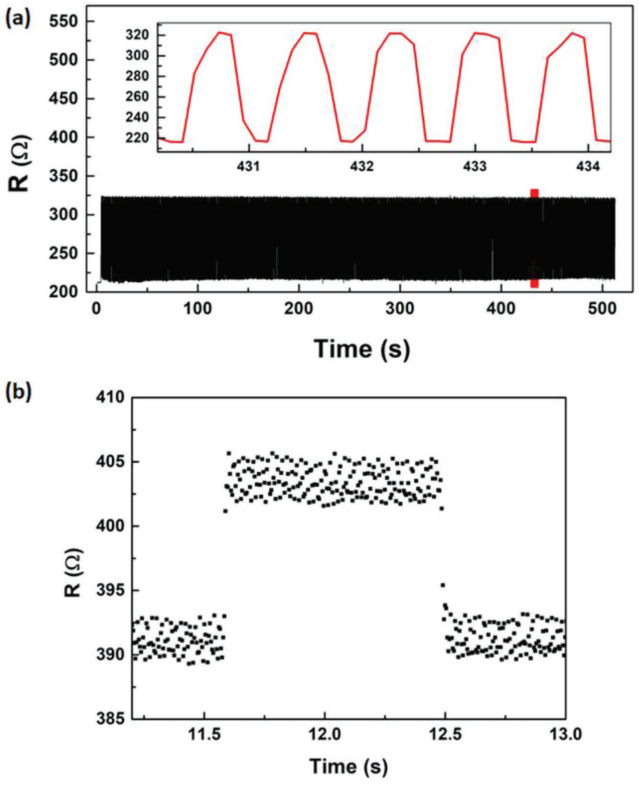

Figure 4. a) Cycling test of the four ribbons patterned VGs film sensor device without PMMA cover. Stable resistance response of about 1000 test cycles is shown. Inset: a close-up view of the curve. b) Typical time-resolved resistance respond curve in fast testing cycles of a 50 μm wide strip array sample. The response time is about 10 ms upon both the strain load and the strain release processes.

During the measurements, a fixed voltage of 20 mV was applied to drive the VGs film strain sensors. As the resistance of our devices typically vary from 50 to 1000 Ω, the power consumption was smaller than 8 μW. With such low operation voltage and power consumption, the devices can be easily driven under practical applications. They can be integrated with the emerging wearable energy supplies, such as the wearable thermoelectric systems,[41,42] and also wearable wireless information transmission systems to realize an all-wearable working system,[43] which is of great convenience in human body related detection.

It should be noticed that the low operation voltage and power consumption are guaranteed by the low square resistance of the VGs film. A typical value of 93.45 Ω $\square^{-1}$ was measured for the VGs film (Figure S12, Supporting Information). As we known, large amount of dislocation, grain boundary, and wrinkles may result in a high square resistance of the film due to the scattering effect.[44,45] As for the VGs film used in our devices, the pregrown buffer layer played an important role to reduce the square resistance.[46] And some of the standing graphene nanosheets might bridge the grain boundaries, wrinkles, and other defects, which further reduced the square resistance of the VGs film.[47]

As all our devices were tested in a two-terminal measurement scheme, it is important to confirm the effect of the contact resistance between the VGs film and the metal electrodes. With a four-terminal testing scheme, we contrast the device performance with and without the effect of resistance of the VGs/metal contact (two-terminal measurement vs four-terminal measurement). As shown in Figure S13a (Supporting Information), linear *IV* curve was measured with a current sweeping from 0 to 2 mA, both in the two- and four-terminal measurement. It is then obvious that, the VGs/metal contact has a linear current–voltage relationship, due to a metal contact between the VGs material and the gold electrodes. Resistance response to applied strain of 0.51% is shown in Figure S13b in the Supporting Information. Better SNR can be obtained with resistance of the VGs/metal contact excluded. And also, about double relative resistance change under the same applied strain can be obtained (Figure S13c, Supporting Information) for the tested device, which indicates a higher sensitivity with contact resistance excluded.

With properties of small detection limit, fast response speed, low operation voltage, and power consumption, our sensor device shows promising potential in human body physiological activity monitoring. Pulses measuring was then taken with sensor device based on the VGs films. To get better fit with the human body, PDMS/VGs film/PDMS sandwiched sensor devices were prepared. With the device placed on the wrist above the radial artery, pulses of an adult human were recorded (**Figure 5**).

As the sensor was placed with the standing nanosheets facing the wrist, when a pulse arises, both the bending and the compacting of the device resulted a compression of the nanosheets. Decrease of the device resistance was then resulted. Similar phenomenon have been reported in earlier works, which was observed with nanographene film.[18] Clear details, which are related to the pulse wave propagation process, can be seen in a single pulse cycle as we colored in red in the figure. The wave shape well matches with valley *P*1 corresponding to the early systolic pressure, and *P*2 to the late systolic pressure. Time delay between *P*1 and *P*2 ($\Delta T_{DVP} = t_{P2} - t_{P1}$, ≈157 ms here),

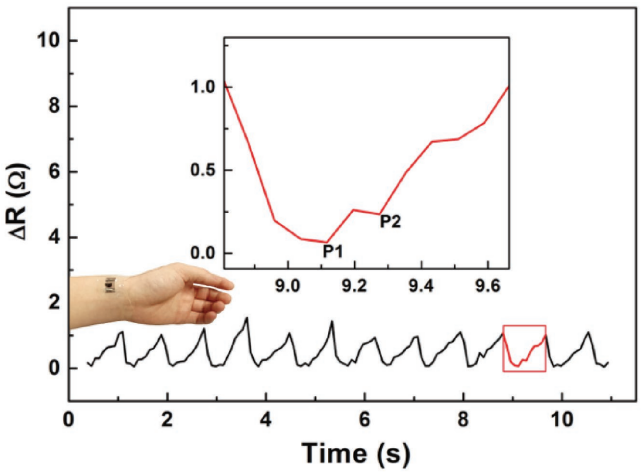

Figure 5. Radial artery pulse signal of a young woman volunteer. Inset: Details of a pulse cycle marked in red and device attached to the wrist for pulse detection.

which is one of the two commonly used parameters to diagnose arterial stiffness,[8,48] can be calculated with these characteristic points. The other parameter, arterial radial augmentation index (AI_r = Pressure(*P*2)/Pressure(*P*1)), might also be calculated with a factor correction of the pressure response of our sensor. Benefiting from the low power consumption and easy processing, the sandwich-structured device offers us a good choice to monitor the arterial pulse wave.

Heart-rate data are consistent with the pulses measured with our device. As for heart rate monitoring, the common used technologies are mainly based on electrocardiography (ECG) sensors consisting of an electrical monitor/transmitter and a receiver, and photoplethysmography (PPG) sensors, which measures changes in blood flow by monitoring light scattering off blood vessels. The ECG sensors usually get signals from the chest. They are not so convenient when compared with our artery pulse monitors. In fact, due to the convenience to realize a daily wearable monitor, artery pulse monitors would be the main choice of the next generation heart rate monitor for daily use.

The PPG sensors have already been used for heart rate monitors included in smartwatches, smart bands, and cell phones. Some of these optical sensors are able to measure blood oxygen saturation in addition. Compared with this major competing technology, a higher signal to noise ratio and possible real-time blood pressure monitoring after a factor correction of the pressure response might be the main advantages of monitors based on strain-induced electrical sensors as presented in this work.

In summary, we demonstrated a high-performance strain sensor based on thermal CVD VGs films. Edges formed by patterning the film into ribbons served as a key factor for the device performance. With new edges introduced, gauge factor of our sensor can reach as high as 150. When more edges were introduced by preparing thinner and denser slices at the same film area, the sensor device showed smaller detection limits. Strain limit as low as 0.07% was detected with VGs film patterned into 200 μm × 200 μm square array. Benefiting from low square resistance (≈93.45 Ω $\square^{-1}$) of the film, the VGs film strain sensor has a low operation voltage (20 mV) and low power consumption (<8 μW), which are big advantages for wearable electronics. To demonstrate the practical application, monitoring of radial arterial pulse wave of a human adult was conducted with PDMS/VGs film/PDMS sandwich sensor devices.

Experimental Section

Device Fabrication Process: The strain sensitive devices were fabricated by locating VGs films onto an IPS (purchased from Obducat) substrate with two-end electrodes prepared in advance (Figure S1, Supporting Information). On top of the IPS substrate, a PDMS (Sylgard 184 purchased from Dow Corning) precursor layer with a thickness of about 100 nm (10:1 ratio of base:curing agent) was spin-coated and then cross-linked at 353 K in vacuum for 90 min. Ti/Au electrodes of 5/45 nm in thickness were deposited onto the PDMS/IPS substrate in thermal evaporation system with prepatterned metal masks. To transfer the VGs film grown on Si or SiO_2 substrate to the electrodes prepared substrate, the sample was first spin-coated with a PMMA layer of 1 μm in thickness, followed by a baking of 453 K for 1 min (Figure S1a, Supporting Information). The Si or SiO_2 substrate was then etched in 15 mol L^{-1} NaOH solution (Figure S1b, Supporting Information), till the

PMMA-coated VGs film floating on the liquid (Figure S1c, Supporting Information). After that, the VGs film was transferred to deionized water to clean the NaOH residual (Figure S1d, Supporting Information) and repeated the process five times. Then the PMMA layer was dissolved in acetone and the VGs film was recleaned in deionized water (Figure S1e, Supporting Information). Finally, the VGs film was carefully placed to connect the two ends of the electrodes (Figure S1f, Supporting Information). A baking of 343 K for 5 min was taken to dry the device. For PMMA covered sensor devices, the VGs films were transferred onto the electrodes without the PMMA dissolving process.

Introducing of Strain and Gauge Factor Calculation: In tests of the device responding, the strain was applied through substrate bending.[18] A homebuilt step-motor-controlled guide stem was used to provide precise relative movement of the two blocks of the sample holder and bending of the PDMS/IPS substrate was then introduced. The moving steps of the step motor can be finally translated to accurate strains through the geometrical relationship. Change of the device resistance was monitored with a semiconductor parameter analyzer during the strain loading and unloading process. Gauge factor can then be calculated with the relative resistance change and the applied strain. More details on the calculation can be found in the Supporting Information.

Fabrication of PDMS/VGs film/PDMS Sandwiched Sensor Device: PDMS precursor and the cross-linking agent were mixed with a ratio of 10:1 and then put in a plastic culture dish to be cured at 353 K for 1.5 h in vacuum chamber. Ti/Au (5/45 nm) electrodes were prepared on cured PDMS with patterned metal mask. VGs film was then placed to connect the two-end electrodes, which were connected out with copper wires and conductive adhesives. Another PDMS layer was placed on the top of the device.

Characterization Methods: The nanostructures of the VGs film were observed by field-emission scanning electron microscopy (FE-SEM) (FEI Helios 600i). The S-shaped electrodes and patterned VGs films were characterized using optical microscope (OLYMPUS MX50). The electrical properties were characterized using a semiconductor parameter analyzer (Keithley 4200SCS).

Supporting Information

Supporting Information is available from the Wiley Online Library or from the author.

Acknowledgements

Q.J. and C.T. contributed equally to this work. This work was supported by the National Natural Science Foundation of China (Grant No. 61390502, 11704402, 61390503, and 11574369), the Strategic Priority Research Program of the Chinese Academy of Sciences (XDB 30000000 and XDB 12030100) and the Ministry of Science and Technology of China (Grant No. 2016YFA0200803).

Conflict of Interest

The authors declare no conflict of interest.

Keywords

flexible electronic devices, health monitoring, RIE patterning, strain sensors, vertically oriented graphene

Received: October 30, 2018
Revised: December 20, 2018
Published online:

[1] H. Sawada, M. Kitani, Y. Hayashi, *Adv. Funct. Mater.* **2014**, *24*, 3299.
[2] J. Kim, M. Lee, H. J. Shim, R. Ghaffari, H. R. Cho, D. Son, Y. H. Jung, M. Soh, C. Choi, S. Jung, K. Chu, D. Jeon, S.-T. Lee, J. H. Kim, S. H. Choi, T. Hyeon, D.-H. Kim, *Nat. Commun.* **2014**, *5*, 5747.
[3] X. Wu, Y. Ma, G. Zhang, Y. Chu, J. Du, Y. Zhang, Z. Zhuo, Y. Duan, Z. Fan, J. Huang, *Adv. Funct. Mater.* **2015**, *25*, 2138.
[4] S. Jung, J. H. Kim, J. Kim, S. Choi, J. Lee, I. Park, T. Hyeon, D.-H. Kim, *Adv. Mater.* **2014**, *26*, 4825.
[5] S. Lee, Y. Inoue, D. Kim, A. Reuveny, K. Kuribara, T. Yokota, J. Reeder, M. Sekino, T. Sekitani, Y. Abe, T. Someya, *Nat. Commun.* **2014**, *5*, 5898.
[6] E. Roh, B.-U. Hwang, D. Kim, B.-Y. Kim, N.-E. Lee, *ACS Nano* **2015**, *9*, 6252.
[7] T. Yang, W. Wang, H. Zhang, X. Li, J. Shi, Y. He, Q. Zheng, Z. Li, H. Zhu, *ACS Nano* **2015**, *9*, 10867.
[8] G. Schwartz, B. C.-K. Tee, J. Mei, A. L. Appleton, D. H. Kim, H. Wang, Z. Bao, *Nat. Commun.* **2013**, *4*, 1859.
[9] R. C. Webb, A. P. Bonifas, A. Behnaz, Y. Zhang, K. J. Yu, H. Cheng, M. Shi, Z. Bian, Z. Liu, Y. S. Kim, W. H. Yeo, J. S. Park, J. Song, Y. Li, Y. Huang, A. M. Gorbach, J. A. Rogers, *Nat. Mater.* **2013**, *12*, 938.
[10] L. Y. Chen, B. C. K. Tee, A. L. Chortos, G. Schwartz, V. Tse, D. J. Lipomi, H. S. P. Wong, M. V. McConnell, Z. Bao, *Nat. Commun.* **2014**, *5*, 5028.
[11] D. H. Kim, N. Lu, R. Ghaffari, Y. S. Kim, S. P. Lee, L. Xu, J. Wu, R. H. Kim, J. Song, Z. Liu, J. Viventi, B. De Graff, B. Elolampi, M. Mansour, M. J. Slepian, S. Hwang, J. D. Moss, S. M. Won, Y. Huang, B. Litt, J. A. Rogers, *Nat. Mater.* **2011**, *10*, 316.
[12] Y. Hattori, L. Falgout, W. Lee, S. Y. Jung, E. Poon, J. W. Lee, I. Na, A. Geisler, D. Sadhwani, Y. Zhang, Y. Su, X. Wang, Z. Liu, J. Xia, H. Cheng, R. C. Webb, A. P. Bonifas, P. Won, J. W. Jeong, K. I. Jang, Y. M. Song, B. Nardone, M. Nodzenski, J. A. Fan, Y. Huang, D. P. West, A. S. Paller, M. Alam, W. H. Yeo, J. A. Rogers, *Adv. Healthcare Mater.* **2014**, *3*, 1597.
[13] X. Fu, Z. Liao, J. Zhou, Y. Zhou, H. Wu, R. Zhang, G. Jing, J. Xu, X. Wu, W. Guo, D. Yu, *Appl. Phys. Lett.* **2011**, *99*, 213107.
[14] Y. Wang, R. Yang, Z. Shi, L. Zhang, D. Shi, E. Wang, G. Zhang, *ACS Nano* **2011**, *5*, 3645.
[15] M. Hempel, D. Nezich, J. Kong, M. Hofmann, *Nano Lett.* **2012**, *12*, 5714.
[16] J. Zhao, G. Wang, R. Yang, X. Lu, M. Cheng, C. He, G. Xie, J. Meng, D. Shi, G. Zhang, *ACS Nano* **2015**, *9*, 1622.
[17] Q. Liu, J. Chen, Y. Li, G. Shi, *ACS Nano* **2016**, *10*, 7901.
[18] J. Zhao, C. He, R. Yang, Z. Shi, M. Cheng, W. Yang, G. Xie, D. Wang, D. Shi, G. Zhang, *Appl. Phys. Lett.* **2012**, *101*, 461.
[19] T. Yamada, Y. Hayamizu, Y. Yamamoto, Y. Yomogida, A. I.-Najafabadi, D. N. Futaba, K. Hata, *Nat. Nanotechnol.* **2011**, *6*, 296.
[20] J. Kuang, L. Liu, Y. Gao, D. Zhou, Z. Chen, B. Han, Z. Zhang, *Nanoscale* **2013**, *5*, 12171.
[21] L. Sheng, Y. Liang, L. Jiang, Q. Wang, T. Wei, L. Qu, Z. Fan, *Adv. Funct. Mater.* **2015**, *25*, 6545.
[22] J. J. Park, W. J. Hyun, S. C. Mun, Y. T. Park, O. O. Park, *ACS Appl. Mater. Interfaces* **2015**, *7*, 6317.
[23] M. Jian, K. Xia, Q. Wang, Z. Yin, H. Wang, C. Wang, H. Xie, M. Zhang, Y. Zhang, *Adv. Funct. Mater.* **2017**, *27*, 1606066.
[24] X. Li, R. Zhang, W. Yu, K. Wang, J. Wei, D. Wu, A. Cao, Z. Li, Y. Cheng, Q. Zheng, R. S. Ruoff, H. Zhu, *Sci. Rep.* **2012**, *2*, 870.
[25] Y. Tang, Z. Zhao, H. Hu, Y. Liu, X. Wang, S. Zhou, J. Qiu, *ACS Appl. Mater. Interfaces* **2015**, *7*, 27432.
[26] W. L. Sang, J. J. Park, B. H. Park, S. C. Mun, T. P. Yong, T. S. Seo, W. J. Hyun, O. O. Park, *ACS Appl. Mater. Interfaces* **2017**, *9*, 11176.
[27] U. H. Shin, D. W. Jeong, S. M. Park, S. H. Kim, H. W. Lee, J. M. Kim, *Carbon* **2014**, *80*, 396.
[28] S. H. Bae, Y. Lee, B. K. Sharma, H. J. Lee, J. H. Kim, J. H. Ahn, *Carbon* **2013**, *51*, 236.

[29] H. Tian, Y. Shu, Y. L. Cui, W. T. Mi, Y. Yang, D. Xie, T. L. Ren, *Nanoscale* **2014**, *6*, 699.
[30] A. Sahlberg, F. Nilsson, A. Berglund, H. Nguyen, K. Hjort, S. H. Jeong, *Adv. Mater. Technol.3*, **2018**, 1700330.
[31] A. Collado, A. Georgiadis, *IEEE Trans. Circuits Syst. I: Reg. Papers* **2013**, *60*, 2225.
[32] L. Roselli, N. B. Carvalho, F. Alimenti, P. Mezzanotte, G. Orecchini, M. Virili, C. Mariotti, R. Goncalves, P. Pinho, *Proc. IEEE* **2014**, *102*, 1723.
[33] J.-H. Bahk, H. Fang, K. Yazawa, A. Shakouri, *J. Mater. Chem. C* **2015**, *3*, 10362.
[34] W.-S. Jung, M.-J. Lee, M.-G. Kang, H. G. Moon, S.-J. Yoon, S.-H. Baek, C.-Y. Kang, *Nano Energy* **2015**, *13*, 174.
[35] A. J. Bandodkar, J. M. You, N. H. Kim, Y. Gu, R. Kumar, A. M. V. Mohan, J. Kurniawan, S. Imani, T. Nakagawa, B. Parish, M. Parthasarathy, P. P. Mercier, S. Xu, J. Wang, *Energy Environ. Sci.* **2017**, *10*, 1581.
[36] H. Wang, E. Gao, P. Liu, D. Zhou, D. Geng, X. Xue, L. Wang, K. Jiang, Z. Xu, G. Yu, *Carbon* **2017**, *121*, 1.
[37] H. Wang, X. B. Li, L. Gao, H. L. Wu, J. Yang, L. Cai, T. B. Ma, C. H. Tung, L. Z. Wu, G. Yu, *Angew. Chem., Int. Ed.* **2018**, *57*, 192.
[38] W. Yu, X. Duan, *Sci. Rep.* **2013**, *3*, 1248.
[39] N. M. Sangeetha, N. Decorde, B. Viallet, G. Viau, L. Ressier, *J. Phys. Chem. C* **2013**, *117*, 1935.
[40] M. B. Coskun, A. Akbari, D. T. H. Lai, A. Neild, M. Majumder, T. Alan, *ACS Appl. Mater. Interfaces* **2016**, *8*, 22501.
[41] Y. Eom, D. Wijethunge, H. Park, S. H. Park, W. Kim, *Appl. Energy* **2017**, *206*, 649.
[42] M. Hyland, H. Hunter, J. Liu, E. Veety, D. Vashaee, *Appl. Energy* **2016**, *182*, 518.
[43] Y. Khan, A. E. Ostfeld, C. M. Lochner, A. Pierre, A. C. Arias, *Adv. Mater.* **2016**, *28*, 4373.
[44] A. A.-Ardakani, A. A. Bol, G. S. Tulevski (IBM), US8853034B2, **2014**.
[45] T. Ma, Z. Liu, J. Wen, Y. Gao, X. Ren, H. Chen, C. Jin, X. Ma, N. Xu, H. Cheng, W. Ren, *Nat. Commun.* **2017**, *8*, 14486.
[46] X. Li, Y. Zhu, W. Cai, M. Borysiak, B. Han, D. Chen, R. D. Piner, L. Colombo, R. S. Ruoff, *Nano Lett.* **2009**, *9*, 4359.
[47] H. Sun, G. Ge, J. Zhu, H. Yan, Y. Lu, Y. Wu, J. Wan, M. Han, Y. Luo, *RSC Adv.* **2015**, *5*, 108044.
[48] W. W. Nichols, *Am. J. Hypertens.* **2005**, *18*, 3.